Available online at www.sciencedirect.com

ScienceDirect

Materials Today: Proceedings 00 (2016) 000–000

materialstoday: PROCEEDINGS

www.materialstoday.com/proceedings

Functional nanomaterials

Diagnose Pathogens in Drinking Water via Magnetic Surface-Enhanced Raman Scattering (SERS) Assay

Hanbing Li[a], Cui Li[a,b], Francis L. Martin[a], Dayi Zhang[a,*]

[a]*Lancaster Environment Centre, Lancaster University, Lancaster LA1 2YQ, UK*
[b]*Key Laboratory of Urban Pollutant Conversion, Institute of Urban Environment, Chinese Academy of Sciences, Xiamen 361021, China*

Abstract

Rapid identification and diagnosis of bacteria and other microorganisms is a great challenge for drinking water safety due to the increasing frequency of pathogenic infections. Raman spectroscopy is a non-destructive tool to characterize the biochemical fingerprints of bacterial cells and its signal can be improved by surface-enhanced Raman scattering (SERS). Thus, Raman scattering has a huge potential in fast diagnosis of pathogens in drinking water, with low cost and high reproducibility. In this work, we developed a novel fast diagnosis method to detect aquatic pathogens via magnetic SERS assay. With chemical co-precipitation synthesis and surface glucose reduction, the silver-coated magnetic nanoparticles (Ag@MNPs) had a well-developed core-shell structure and high efficiency to capture bacterial cells. Ag@MNPs achieved 10^3 enhancement factor for rhodamine 6G and the limit of detection was 10^{-9} M. The magnetic SERS assay also successfully detected various bacteria (*A. baylyi* and *E. coli*) with high sensitivity (10^5 CFU/mL). This platform provided a promising and easy-operation approach for pathogen detection for food and drinking water safety.

Selection and Peer-review under responsibility of the Conference Committee Members of Functional Nanomaterials in Industrial Applications.

Keywords: magnetic nanoparticles (MNPs); silver-coated MNPs (Ag@MNPs); Raman spectroscopy; surface-enhanced Raman scattering (SERS)

* Corresponding author. Tel.: +44-152-451-0288; fax: +44-152-451-0082.
E-mail address: d.zhang@lancaster.ac.uk

Selection and Peer-review under responsibility of the Conference Committee Members of Functional Nanomaterials in Industrial Applications.

1. Introduction

Millions of cases of diseases are caused by pathogens in drinking water [1, 2], though they exist at low concentration and are hard to identify. Many diagnosis methods therefore are developed to rapidly detect these pathogens [3], as polymerase chain reaction (PCR) [4, 5], colony forming [6] and staining [7], but the majority of them are time-consuming and not suitable for worldwide application in practice. It raises great chances for novel technical development for water resource protection and water treatment to rapidly recognize aquatic pathogens addressing drinking water safety issues.

Magnetic nanoparticles (MNPs) have been widely applied in biological science for its affinity to biological molecules [8], such as bioenergy recovery [9], drug delivery [10] and drinking water purification [11]. In environmental science, most relative research has addressed the magnetisms improvement [12, 13] or surface modification to enhance bacteria capturing efficiency [14]. There is limited work on how to use MNPs as a diagnosis tool in quantifying pathogens in drinking water.

Raman microspectroscopy is a promising method for bacterial detection [15]. To improve the signal intensity, surface-enhanced Raman scattering (SERS) was developed [16] and used in diagnosis of pathogens in drinking water [17]. However, direct application of SERS requires the mixture and separation of bacterial cells with suspended Ag/Au nanoparticles [18] or bacteria capture on mesostructured materials supported with Ag/Au nanoparticles [19]. The former approach suffers from the difficulties in recovering Ag/Au nanoparticles from the samples, and the latter one faces the challenges that the low cell counts in water samples means the low capture efficiency. Considering the magnetic enrichment of MNPs and SERS active substrate Ag/Au, some surface modification has been applied to combine these two types of nanomaterials together in detecting pollutants [20], biomarkers [21] or pathogens [22].

Here, we developed a novel high-sensitive screening method for rapid detection of pathogens in drinking water with silver-coated MNPs (Ag@MNPs) by magnetic capturing and SERS diagnosis. The limit of detection for bacteria was significantly improved, attributing to the magnetic enrichment and SERS signal enhancement which were simultaneously achieved by Ag@MNPs.

2. Experimental Section

2.1. Synthesis of silver coated magnetic nanoparticles

The synthesis of MNPs followed chemical co-precipitation [23] and Ag surface coating was achieved by glucose reduction (Mandal et al., 2005; Sau & Murphy, 2004). Briefly, 1.0 M $FeCl_3$ (2.0 mL in 1.0 M HCl) and 2.0 M $FeCl_2$ (0.5 mL in 1.0 M HCl) were mixed and homologized, with 25 mL NaOH (2.5 M) dropwisely added until the appearance of dark iron oxide precipitates. With further 30 min vortex, the iron oxide suspension was separated by permanent magnet and washed by deionized water until neutral pH. The synthesized MNPs were further coated with silver as SERS active substrate by mixing 1 mL MNPs with a proper weight of Ag_2SO4 to reach a 1:20 (MNPs:Ag_2SO4) molar ratio. After adding 0.5 g glucose and sonicated for 15 min, the suspension was heated to 80 ℃ in a water bath and slowly stirred for 1 hour. The MNPs turned from dark into brownish colour, and the Ag@MNPs were further stirred for 30 minutes until room temperature. Separated by permanent magnet and washed by deionized water, Ag@MNPs were stored for further experiment and analysis.

2.2. Bacterial strains and cultivation

In this study, the two bacterial strains were *Acinetobacter baylyi* ADP1 and *Escherichia coli* JM109, with close phylotypic relationship to clinical pathogens *Acinetobacter baumannii* and *Escherichia coli* O157:H7. The strains were grown in sterile Lysogeny Broth medium for 16 hours, at 30 ℃ for *A. baylyi* and 37 ℃ for *E. coli*, respectively. The cell suspensions were further centrifuged at 4,000 rpm for 5 min and washed three times by sterile deionized water. Afterwards, the bacterial cells were serially diluted to 10^8 CFU/mL and 10^5 CFU/mL for Raman microspectroscopy analysis.

2.3. Bacteria capture and Raman microspectroscopy analysis

By adding the MNPs or Ag@MNPs suspension (5 μL) into diluted cell suspension or rhodamine 6G (R6G) samples (1 mL), the mixture was cultivated for 10 min and the magnetic pellets were harvested by permanent magnet. The pellet was then washed by deionized water and ethanol five times for Raman microspectroscopy analysis, obtained by InVia Raman microscopy (Horiba, UK) with 785-nm excitation laser (100% and 1% power for normal Raman and SERS spectrum respectively), 10 second exposure time and a 500-2000 cm^{-1} spectral range. For all the spectral measurement, at least twenty biological replicates were randomly selected and analysed.

2.4. Chemical and biological analysis

The phase identification of synthesized MNPs and Ag@MNPs nanocomposites was carried out by X-ray diffraction (XRD, D8-Advance, Bruker, UK). The magnetic properties were measured by a vibrating sample magnetometer (VSM, Lake Shore, 7304, USA) at 25℃ and in a magnetic field varying from -1.7 T to +1.7 T. The Raman spectra were first subtracted by the IRootLab Matlab interface for spectra truncation between 500-2000 cm-1 and baseline correction (Martin et al., 2010). The Raman signal intensity of R6G was calculated at the bands of 1514, 1365, 1310, 1184, 774 and 614 cm^{-1}. To calculate the capture efficiency of MNPs and Ag@MNPs towards bacteria cells, the number of total and magnetic-free bacteria was determined by quantitative polymerase chain reaction (qPCR) respectively according to our previous study (Zhao et al., 2016). The 16S rRNA primer pair was 341F (5'-CCTACGGGNGGCWGCAG-3') and 802R (5'-TACNVGGGTATCTAATCC-3'). Each 10 μL qPCR reaction system contained 1 μL of each primer, 1 μL DNA template, 2 μL molecular water and 5 μL iTaq™ Universal SYBR® Green Supermix (BioRad, USA). The thermos cycling parameters followed: 94℃ for 3 min; 34 cycles of 94℃ for 45 s, 52℃ for 45 s, 72℃ for 45 s and 80℃ for 15 s for fluorescence data acquisition. Standard curves were obtained with serial dilutions of quantified plasmid DNA containing the fragment of 16S rRNA.

3. Results and Discussion

3.1. Characterization of silver-coated magnetic nanoparticles

The XRD pattern (Fig. 1a) identified the diffraction peaks of synthesized MNPs as 2θ=30.0°, 35.4°, 43.2°, 53.6°, 57.1° and 62.7°, indexed to (220), (311), (400), (422), (511) and (440) lattice planes [24]. For Ag@MNPs, the key diffraction peaks were 2θ=38.1°, 44.3° and 64.4°, indexed to (111), (200) and (220) lattice planes [25]. The characteristic diffraction peaks of pure MNPs were significantly weakened and hardly distinguished on Ag@MNPs (black triangle in Fig. 1a). The results proved that Ag@MNPs nanocomposites had a well core-shell structure with fine Ag-coating on MNPs surface. Our magnetization test further illustrated that both the magnetization curves behaved the *S* shape (Figure 1b). The highest saturation magnetization of MNPs and Ag@MNPs was 44.3 emu/g and 37.9 emu/g respectively. It was worth mentioning that the magnetic separation of MNPs and Ag@MNPs were similar, and both supernatants were completely transparent. These results indicated limited magnetism loss after Ag-coating and the strong magnetic harvesting capacity of Ag@MNPs, suggesting that Ag@MNPs could be effectively controlled by magnetic field.

Ag@MNPs maintained high capture efficiency for bacterial cells (Fig. 2). From the results of qPCR, the original concentration of *E. coli* and *A. baylyi* suspension was 1.03×10^{9} CFU/mL and 1.79×10^{8} CFU/mL, respectively. After magnetic separation by MNPs and Ag@MNPs, the amount of magnetic-free bacteria in the supernatant was 5.0×10^{4} CFU/mL (MNPs) and 17.6×10^{4} CFU/mL (Ag@MNPs) for *E. coli*, and 4.6×10^{4} CFU/mL (MNPs) and 2.8×10^{4} CFU/mL (Ag@MNPs) for *A. baylyi*, respectively. The capture efficiency of MNPs and Ag@MNPs were both higher than 99.5% for *E. coli* and 99.9% for *A. baylyi*. Such similar capture efficiency indicated that: 1) Ag-coating showed limited impacts on the surface electrostatic properties of MNPs and the electrostatic attraction was attributed to the positively charged MNPs towards negative bacterial cells; 2) Ag@MNPs capturing was non-selective and could be used for various bacterial strains. Different from previous research which employed polymers to achieve high bacteria capture efficiency [8], our method directly coated Ag on naked MNPs and minimized the disturbance

of coating polymers on SERS signal. Besides, we did not introduce silicon dioxide shell for surface Ag- or Au-coating [26] and therefore maintained the high magnetism and strong affinity to bacteria of Ag@MNPs. Meanwhile, Ag@MNPs were not further functionalized with antibody conjugation to target specific bacteria as previous study [27, 28]. It broadened the application area of this magnetic assay for all types of pathogen detection in drinking water by direct electrostatic attraction. Given these advantages, the Ag@MNPs assay was therefore easy to be used for bacteria capture and magnetic enrichment for further SERS analysis.

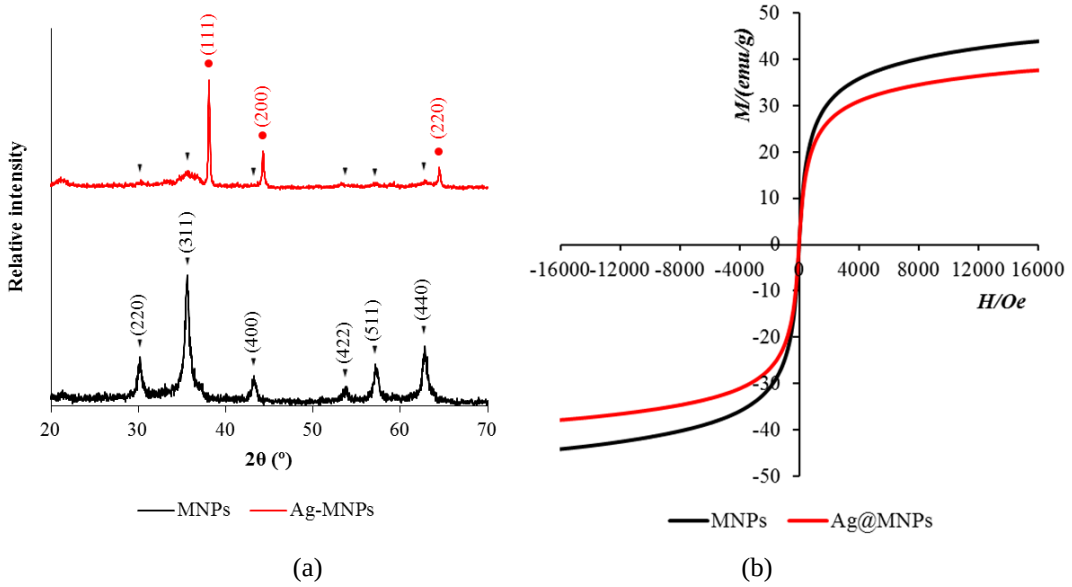

Fig. 1. The XRD pattern (A) and magnetization curve (B) of MNPs and Ag@MNPs nanocomposites.

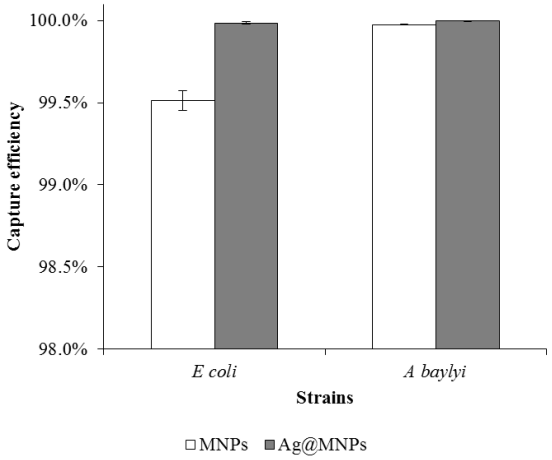

Fig. 2. Bacteria capture efficiency of MNPs and Ag@MNPs.

3.2. SERS enhancement of Ag@MNPs

Strong and stable SERS signal was obtained in the treatment of R6G with Ag@MNPs, proving the SERS enhancement by Ag@MNPs nanocomposite, as illustrated in Fig. 3a. Since R6G is a fluorescent xanthene derivative that possesses strong Raman effect when excitation laser emitting into its adsorption band [29], it was employed here to validate the enhancement of Ag@MNPs on Raman scattering. The predominant Raman shifts of R6G were

at 1185, 1498, 1367 and 1310 cm^{-1} attributing to in-plane C-C stretch vibrations, 611 cm^{-1} for C-C-C ring in-plane bend vibrations, and 772 cm^{-1} for C-H out-of-plane bend vibrations [30]. The Raman spectra intensities of R6G characteristic peaks with 100% laser power excitation ranged from 1390.28 (611 cm^{-1}) to 4238.28 at (1365 cm^{-1}) when R6G concentration was 10^{-6} M. Treated with Ag@MNPs, strong SERS signals were identified with only 1% laser power. The six key Raman shift peaks included 611, 772, 1185, 1295, 1367 and 1498 cm^{-1}, similar to normal R6G Raman spectra. Different from conventional SERS analysis dropping R6G onto SERS active substrates [31], we directly mixed R6G with Ag@MNPs suspension and allowed their interaction in aquatic phase. The harvesting of Ag@MNPs via permanent magnet significantly concentrated R6G on the magnetic spot to achieve strong SERS signal. The Raman signal enhancement of Ag@MNPs was evaluated by the enhancement factor (EF), as calculated by Equation (1):

$$EF=I_{SERS}/I_{Normal} \quad (1)$$

where I_{SERS} is the Raman signal intensities of R6G with Ag@MNPs at 1% laser power; I_{Normal} is Raman signal intensities of 10^{-6} M pure R6G at 1% laser power.

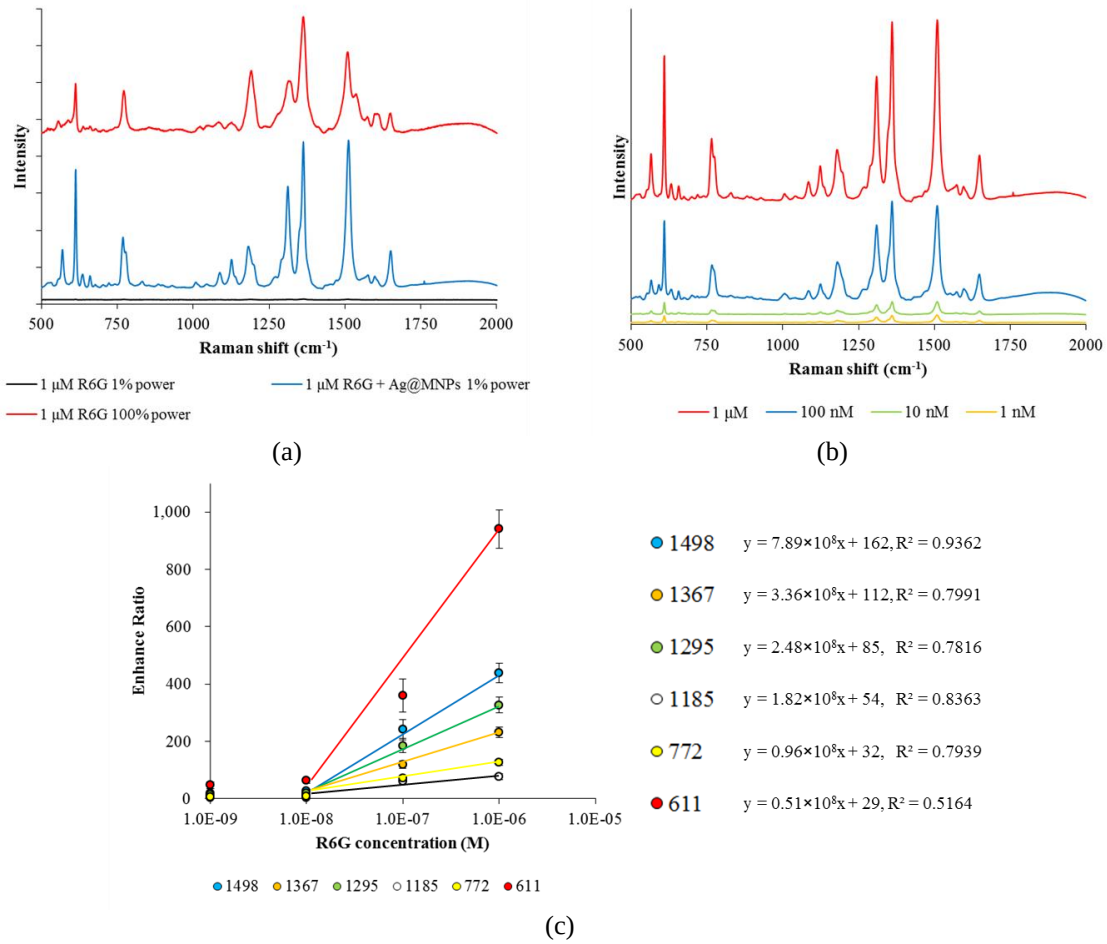

Fig. 3. R6G SERS spectra with Ag@MNPs. (a) Raman spectra of pure R6G and R6G with Ag@MNPs. (b) R6G SERS spectra of different concentrations. (c) Calibration curve of R6G SERS intensity.

For all the tested R6G concentrations (10^{-9} to 10^{-6} M), strong SERS signals were detected (Fig. 3b). For instance, the Raman intensity of 10^{-6} M R6G with Ag@MNPs with 1% laser power was about 1.5 times higher than that of

10^{-6} M pure R6G with 100% laser power. We therefore proved that Ag@MNPs were SERS active substrates. From the calculation, the Raman signal of peak 611 cm^{-1} was enhanced nearly 10^3 times by Ag@MNPs when R6G concentration was 10^{-6} M, followed by 1498 cm^{-1} (439 times), 1295 cm^{-1} (327 times), 1367 cm^{-1} (232 times), 772 cm^{-1} (127 times) and 1185 cm^{-1} (77 times). As illustrated in Fig. 3c, the SERS intensity of each characteristic peak was positively correlated with the R6G concentrations, with a quantitative range from 10^{-8} M to 10^{-6} M. The limit of detection of R6G SERS with magnetic Ag@MNPs assay was 10^{-9} M, when the enhancement factor was 15 and distinguishable from the background, although the peaks of 772 cm^{-1} and 1185 cm^{-1} were non-detectable.

3.3. In situ bacteria detection by SERS

Different from conventional SERS detecting bacteria, we developed a magnetic SERS assay for the rapid screening of bacterial cells in aquatic phase. The Ag-coating did not affect the electrostatic interaction between MNPs and bacteria, allowing the non-selective capture and further enrichment by magnet. The bacteria were detected and quantified by the sensitive plasmonic Ag@MNPs SERS.

Bacterial SERS spectra varied from spot to spot due to the heterogeneous distribution of Ag@MNPs and bacterial cells at low concentration. The SERS spectra of individual cells were then randomly collected and the results demonstrated its high reproducibility. Fig. 4 showed the significant enhancement of Raman signal by Ag@MNPs assay. With 1% laser power, the enhancement factor of Ag@MNPs was similar for *E. coli* and *A. baylyi*, around 50-100 times compared to pure bacterial cells. It was significantly lower than that of R6G (10^2 to 10^3 as discussed above), attributing to the complicated structure and different functional groups of bacterial cell membrane. The main SERS shifts of *A. baylyi* and *E. coli* included 660, 731, 964, 1210, 1251, 1325 and 1584 cm^{-1}. The band with the highest SERS intensity was 731 cm^{-1}, explained by the ring breathing of adenine. The bands at 1210 and 1251 cm^{-1} were caused by Amide III of proteins [32]. The band at 1325 cm^{-1} was contributed not only from nucleic acid bases adenine and guanine, but also from aromatic amino acid tyrosine [33, 34]. Ring stretch vibration led to the band at 1584 cm^{-1} which was weaker than the other SERS peaks [35]. For the band at 964 cm^{-1}, previous studies tentatively assigned it to the C-N stretch [36]. Meanwhile, the band at 660 cm^{-1} is construed as a discriminative peak of guanosine in bacterial SERS spectra [34].

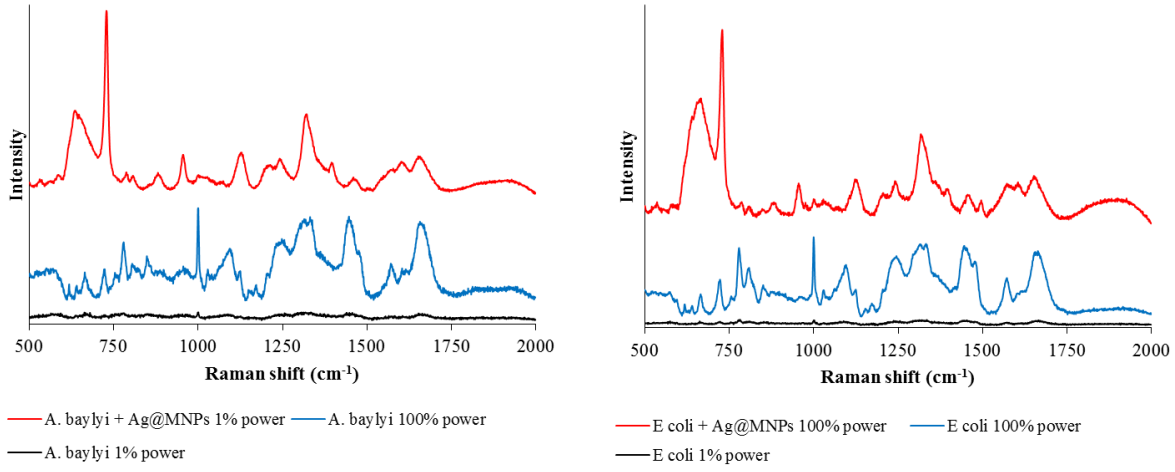

Fig. 4. Raman and SERS spectra of bacteria. (a) for *A. baylyi* and (b) for *E. coli*.

Compared to normal Raman spectra of *A. baylyi* and *E. coli*, we found different Raman spectra profiles of Ag@MNPs SERS. For instance, the most obvious band for normal Raman spectra of both bacteria was 1003 cm^{-1} attributing to polysaccharide [17], which was not enhanced by Ag@MNPs. It might be explained by the favourable binding of Ag@MNPs to some specific extracellular molecules [37], such as adenine and guanine. Meanwhile, the SERS spectra changed slightly at different bacterial concentration, explained by the change from sub-monolayer

coverage to full monolayer coverage [38]. Thus, the SERS intensity and characteristic bands of bacteria via Ag@MNPs might be used to quantify bacterial concentration. In the present work, the direct limited of bacteria detection via normal Raman in aquatic phase was 10^8 CFU/mL, while it was significantly improved to 10^5 CFU/mL when magnetically captured and enriched by Ag@MNPs.

4. Conclusion

For the first time in this study, we proposed and proved the novel concept of capturing bacteria from drinking water and fast detecting their concentration via SERS on magnetic-controllable Ag@MNPs. The results indicated that the bacterial cells were effectively captured by Ag@MNPs and then magnetically enriched for SERS analysis. The Raman intensity was enhanced 10^2-10^3 times when R6G was used as the standard chemical and the limit of detection was 10^{-9} M with SERS active substrate Ag@MNPs. This magnetic SERS assay achieved high sensitivity (10^5 CFU/mL) and rapid screening (<15 min) to diagnose bacteria in water samples. With further fabrication and instrumentation, this technique provides opportunities in diagnosing pathogens in other environmental or clinical samples.

Acknowledgement

The authors would like to thank National Natural Science Foundation of China (No. 41301331) for financial support. The authors are thankful to Chinese Scholarships Council (CSC) for providing studentship.

References

[1] U. Szewzyk, R. Szewzyk, W. Manz, K.H. Schleifer, *Annu. Rev. Microbiol.*, 54 (2000) 81-127.
[2] World Health Organization. 2011. *Guidelines for drinking-water quality. Fourth ed*. WHO Library Cataloguing-in-Publication Data.
[3] A. Rompre, P. Servais, J. Baudart, M.R. de-Roubin, P. Laurent, *J. Microbiol. Methods*, 49 (2002) 31-54.
[4] A.M. Ibekwe, P.M. Watt, C.M. Grieve, V.K. Sharma, S.R. Lyons, *Appl. Environ. Microbiol.*, 68 (2002) 4853-4862.
[5] U. Dharmasiri, M.A. Witek, A.A. Adams, J.K. Osiri, M.L. Hupert, T.S. Bianchi, D.L. Roelke, S.A. Soper, *Anal. Chem.*, 82 (2010) 2844-2849.
[6] V.T.C. Penna, S.A.M. Martins, P.G. Mazzola, *BMC Public Health*, 2 (2002).
[7] M.J. Lehtola, C.J. Loades, C.W. Keevil, *J. Microbiol. Methods*, 62 (2005) 211-219.
[8] Y.-F. Huang, Y.-F. Wang, X.-P. Yan, *Environ. Sci. Technol.*, 44 (2010) 7908-7913.
[9] Z. Lin, Y. Xu, Z. Zhen, Y. Fu, Y. Liu, W. Li, C. Luo, A. Ding, D. Zhang, *Bioresour. Technol.*, 190 (2015) 82-88.
[10] C. Sun, J.S.H. Lee, M. Zhang, *Adv. Drug Delivery. Rev.*, 60 (2008) 1252-1265.
[11] Y. Xu, C. Li, X. Zhu, W.E. Huang, D. Zhang, *Environ. Eng. Manage. J.*, 13 (2014) 2023-2029.
[12] I. Ennen, C. Albon, A. Weddemann, A. Auge, P. Hedwig, F. Wittbracht, A. Regtmeier, D. Akemeier, A. Dreyer, M. Peter, P. Jutzi, J. Mattay, N. Mitzel, N. Mill, A. Hutten, *Acta Phys. Pol. A*, 121 (2012) 420-425.
[13] C. Ozdemir, O. Akca, E.I. Medine, D.O. Demirkol, P. Unak, S. Timur, *Food Anal. Meth.*, 5 (2012) 731-736.
[14] J. Luis Corchero, A. Villaverde, *Trends Biotechnol.*, 27 (2009) 468-476.
[15] J.W. Chan, A.P. Esposito, C.E. Talley, C.W. Hollars, S.M. Lane, T. Huser, *Anal. Chem.*, 76 (2004) 599-603.
[16] M.D. Porter, R.J. Lipert, L.M. Siperko, G. Wang, R. Narayanana, *Chem. Soc. Rev.*, 37 (2008) 1001-1011.
[17] R.M. Jarvis, R. Goodacre, *Anal. Chem.*, 76 (2004) 40-47.
[18] A.E. Grow, L.L. Wood, J.L. Claycomb, P.A. Thompson, *J. Microbiol. Methods*, 53 (2003) 221-233.
[19] H. Wang, Y. Zhou, X. Jiang, B. Sun, Y. Zhu, H. Wang, Y. Su, Y. He, *Angew. Chem. Int. Edit.*, 54 (2015) 5132-5136.
[20] Q. An, P. Zhang, J.-M. Li, W.-F. Ma, J. Guo, J. Hu, C.-C. Wang, *Nanoscale*, 4 (2012) 5210-5216.
[21] T. Yang, X. Guo, H. Wang, S. Fu, Y. Wen, H. Yang, *Biosens. Bioelectron.*, 68 (2015) 350-357.
[22] L. Zhang, J. Xu, L. Mi, H. Gong, S. Jiang, Q. Yu, *Biosens. Bioelectron.*, 31 (2012) 130-136.
[23] D. Zhang, R.F. Fakhrullin, M. Ozmen, H. Wang, J. Wang, V.N. Paunov, G. Li, W.E. Huang, *Microbial Biotech.*, 4 (2011) 89-97.
[24] X. Zhao, H. Li, A. Ding, G. Zhou, Y. Sun, D. Zhang, *Mater. Lett.*, 163 (2016) 154-157.
[25] J.A. López Pérez, M.A. López Quintela, J. Mira, J. Rivas, S.W. Charles, *J. Phy. Chem. B*, 101 (1997) 8045-8047.
[26] J. Shen, Y. Zhu, X. Yang, J. Zong, C. Li, *Langmuir*, 29 (2013) 690-695.
[27] J. Joo, C. Yim, D. Kwon, J. Lee, H.H. Shin, H.J. Cha, S. Jeon, *The Analyst*, 137 (2012) 3609-3612.
[28] Y.W. Chu, D.A. Engebretson, J.R. Carey, *J. Biomed. Nanotechnol.*, 9 (2013) 1951-1961.
[29] A.M. Michaels, M. Nirmal, L.E. Brus, *J. Am. Chem. Soc.*, 121 (1999) 9932-9939.
[30] P. Hildebrandt, M. Stockburger, *J. Phy. Chem.*, 88 (1984) 5935-5944.
[31] S. Nie, S.R. Emory, *Science*, 275 (1997) 1102-1106.
[32] H. Tian, G. Zhuang, A. Ma, C. Jing, *J. Microbiol. Methods*, 89 (2012) 153-158.
[33] E.C. López-Díez, R. Goodacre, *Anal. Chem.*, 76 (2004) 585-591.
[34] L. Cui, P. Chen, B. Zhang, D. Zhang, J. Li, F.L. Martin, K. Zhang, *Water Res.*, 87 (2015) 282-291.

[35] B. Giese, D. McNaughton, *Phys. Chem. Chem. Phys.*, 4 (2002) 5171-5182.
[36] L. Cui, P. Chen, S. Chen, Z. Yuan, C. Yu, B. Ren, K. Zhang, *Anal. Chem.*, 85 (2013) 5436-43.
[37] M. Kahraman, K. Keseroglu, M. Culha, *Appl. Spectrosc.*, 65 (2011) 500-506.
[38] H.W. Cheng, S.Y. Huan, R.Q. Yu, *The Analyst*, 137 (2012) 3601-8.